A BAYESIAN PROBABILISTIC APPROACH FOR STRUCTURE DAMAGE DETECTION

HOON SOHN * and KINCHO H. LAW †
Department of Civil Engineering, Stanford University, Stanford, CA 94305-4020,*U.S.A.*

SUMMARY

A Bayesian probabilistic approach is presented for the damage detection of multistory frame structures. In this paper, a Bayesian probabilistic approach is applied to identify multiple damage locations using estimated modal parameters when (1) the measurement data are potentially corrupted with noise, (2) only a small number of degrees of freedom are measured, and (3) a few fundamental modes are estimated. To reduce the potentially intensive computational cost of the proposed method, a branch-and-bound search scheme is proposed and a simplified approach for the modeling of multistory frame structures is employed. A six story shear frame example and two multistory frame examples, with multiple damage locations, are presented to illustrate the applicability of the proposed approach.

KEY WORDS: damage detection; Bayesian probabilistic approach; branch-and-bound search; modal parameters; multistory frame structures

1 INTRODUCTION

The ability to monitor the health of building structures is an important activity for the maintenance of a facility. With recent advances in damage detection, the monitoring of a structure is within the capability of current technology. Damage detection methods can be classified into *model based* and *non-model based* methods [14]. Model based damage detection methods locate and quantify damage by correlating an analytical model with test data of the damaged structure. Non-model based methods assess damage by comparing measurements from the undamaged and damaged structures. Model based methods can provide quantitative information of damage as well as damage locations. However, these methods are computationally intensive and require a finite element (FE) model, which is carefully refined with test data of the undamaged structure. While non-model based methods are simple and straightforward, these methods generally do not provide quantitative information about structural damage. The proposed method is a model based method and uses modal vibration test data to characterize the state of the structure. Typically, the procedure for model based damage detection includes four basic steps:

1. Model construction: construct an analytical model and identify structural parameters which closely represent the structure.
2. Modal testing: estimate modal parameters, i.e. the natural frequencies and the modal vectors, corresponding to the current state of the structure.

*Graduate Student, email: sohnhoon@leland.stanford.edu
†Professor, email: law@ce.stanford.edu

3. Damage localization: locate the most likely damaged regions using the estimated modal parameters.
4. Damage assessment and system updating: assess the severity of damage and update the system parameters.

Model updating and parameter estimation techniques have been developed to improve the analytical model using estimated modal data [22, 16, 15]. For damage detection, the analytical model refined by the parameter estimating techniques can be employed as the initial model of the undamaged structure. However, differences between the actual response of the structure and the theoretical response of the analytical model are unavoidable even after the refinement. The differences arise mainly from two types of uncertainties. The first type of uncertainty is due to the presence of noise in the measurements during vibration tests. The second type of uncertainty is the modeling error which arises from the assumptions and simplifications made during the modeling process [18]. Many damage detection methods assume that the initial analytical model is identical to the structure before any damage occurrence [25, 17, 3, 11, 19, 20]. The framework of the proposed method explicitly takes into account the modeling error as well as the measurement noise.

There are two common modal testing procedures, ambient and forced vibration tests. A thorough comparison of ambient and forced vibration tests can be found in Reference [8]. Ambient vibration tests measure dynamic responses during the normal operation of a structure, and can be easily repeated to collect modal data sets. One difficulty with ambient tests is that the conventional frequency response function analysis techniques may not be employed because the forcing function is often unknown. Recently developed system identification techniques are able to estimate modal parameters from ambient vibration tests [8, 4]. Forced vibration tests are performed by imposing a known excitation on the structure. Forced vibration tests are generally performed under closely controlled conditions and, consequently, provide more informative data than those obtained by ambient tests. The time and effort required for forced vibration tests are, however, much greater than those for ambient tests. This study focuses on the development of a damage detection method that can be employed in conjunction with an on-line monitoring system [23]. Since an automated monitoring system for a large civil structure will most likely use ambient excitation, we assume that experimental modal data can be accumulated by ambient vibration tests. To best utilize the accumulated data, we employ a Bayesian probabilistic approach as a heuristic means to combine previous experimental data with newly available test data. Bayesian probabilistic approaches have been applied to damage detection problems by previous researchers [3, 2, 9]. To reduce the potentially intensive computational cost of a Bayesian approach, this paper employs a branch-and-bound search scheme and a simplified approach for the modeling of multistory frame structures.

For damage localization and assessment, residual force vectors (also known as damage vectors or dynamic residual forces) have been employed to locate the most likely damaged regions which are mathematically expressed in terms of degrees of freedom (DOFs) in the analytical model [6, 19, 25]. For the calculation of residual force vectors, the DOFs in the analytical model should coincide with those in the estimated modal vectors. When

only a small number of sensors are installed, one can use either system condensation techniques or modal expansion techniques. System condensation techniques reduce the DOFs defined in the analytical model to the measured DOFs. Reduction techniques often produce a condensed matrix that does not resemble the member connectivity of the original model. As a result, locating damaged members from the residual force vectors of the reduced system becomes very difficult [5, 10]. An alternative is to expand the modal vectors, based on the measurements at the instrumented DOFs, to the size of the analytical model [21, 13]. Modal expansion methods generally do not produce the results that are accurate enough to provide reliable information about damaged DOFs or damaged structural members.

Instead of employing residual force vectors, we search for the most probable damage locations by comparing the relative probabilities for different damage events. The relative probability of a damage event is expressed in terms of the posterior probability of the damage event, given the estimated modal data sets from the structure. In the proposed method, the formulation of the relative posterior probability is based on the modal output error, which is defined as the difference between the estimated modal parameters and the theoretical modal parameters from the analytical model. Using an output error approach, we avoid the aforementioned problems introduced by either modal expansion or reduction techniques.

This paper is organized as follows: The next section describes the theoretical formulation of the Bayesian probabilistic approach. Section 3 presents numerical examples to illustrate the effectiveness of the proposed method. Section 4 summarizes this paper and discusses future work.

2 THEORETICAL FORMULATION

This section presents a damage detection method based on a Bayesian probabilistic approach. First, explicitly considering both modeling and noise errors, we formulate the relative posterior probability of an assumed damage event, which can include multiple substructures as damaged. For the assumed damage locations, the most likely amount of damage is also determined during the calculation of the relative posterior probability. Second, we apply a branch-and-bound search scheme to identify the most likely damage event without searching through all possible damage events. Third, to simplify three dimensional multistory frame analyses, a modeling technique based on the rigid floor diaphragm assumption is employed and extended for damage detection.

2.1 Notations and Assumptions

For an analytical model of a structure, we represent the system stiffness matrix $\mathbf{K}$ as an assembly of substructure stiffness matrices. For a model with N_{sub} substructures, the overall stiffness matrix can be expressed as:

$$\mathbf{K}(\Theta) = \sum_{i=1}^{N_{sub}} \theta_i \mathbf{K}_{si} \tag{1}$$

where $\mathbf{K}_{si}$ is the stiffness matrix of the ith substructure and θ_i $(0 \leq \theta_i \leq 1)$ is a nondimensional parameter which represents the contribution of the ith substructure stiffness

to the system stiffness matrix. The nondimensional parameter θ_i is introduced to allow the modeling of damage in the ith substructure. A substructure is said to have damaged when the θ value is less than a specified threshold. As damage locations and amount are determined according to the θ values, the system stiffness matrix in Equation (1) is expressed as a function of $\Theta = \left\{\theta_i; i = 1, ..., N_{sub}\right\}$.

Modal data sets are assumed to be collected and estimated from repeated or continuous vibration tests. When vibration tests are repeated N_s times, the total collection of N_s modal data sets is denoted as:

$$\hat{\Psi}_{N_s} = \left\{\hat{\psi}(n) \ : \ n = 1, ..., N_s\right\} \tag{2}$$

A modal data set $\hat{\psi}(n)$ in Equation (2) consists of both the frequencies and the modal vectors estimated from the nth vibration test, i.e.,

$$\hat{\psi}(n) = \left[\hat{\omega}_1^n, ..., \hat{\omega}_{N_m}^n, \hat{\mathbf{v}}_1^{nT}, ..., \hat{\mathbf{v}}_{N_m}^{nT}\right]^T \in \mathbf{R}^{N_t} \tag{3}$$

where $\hat{\omega_i^n}$ and $\hat{\mathbf{v}}_i^n$ respectively denote the ith estimated frequency and modal vector in the nth data set. The modal vector $\hat{\mathbf{v}}_i^n$ ($\hat{\mathbf{v}}_i^n \in \mathbf{R}^{N_d}$) has components corresponding to the instrumented DOFs. The variables N_t, N_d and N_m represent the total number of components in a data set $\hat{\psi}(n)$, the number of the measured DOFs and the number of measured modes, respectively.

Let H_j denote a hypothesis for a damage event which can contain any number of substructures as damaged, and the initial degree of belief about the hypothesis H_j is represented with a prior probability $P(H_j)$. Using Baye's theorem, the posterior probability $P(H_j|\hat{\Psi}_{N_s})$, after observing a set of estimated modal parameters $\hat{\Psi}_{N_s}$, can be represented as:

$$P(H_j|\hat{\Psi}_{N_s}) = \frac{P(\hat{\Psi}_{N_s}|H_j)}{P(\hat{\Psi}_{N_s})} P(H_j) \tag{4}$$

The most likely damaged substructures are the ones included in the hypothesis H_{max} which has the largest posterior probability, i.e.

$$P(H_{max}|\hat{\Psi}_{N_s}) = \max_{\forall H_j} P(H_j|\hat{\Psi}_{N_s}) \tag{5}$$

Since the objective is to determine the most probable damage hypothesis, the relative posterior probabilities of alternative hypotheses are of interest. We attempt to avoid the explicit expression of a posterior probability $P(H_j|\hat{\Psi}_{N_s})$ and the examination of all hypotheses. The precise calculation of $P(\hat{\Psi}_{N_s}|H_j)$ is a difficult task. Furthermore, the calculation of the denominator $P(\hat{\Psi}_{N_s})$ in Equation (4) involves summing $P(\hat{\Psi}_{N_s}|H_j) \cdot P(H_j)$ over every possible hypothesis. The number of all possible damage events (the size of hypothesis space) for a structure with N_{sub} substructures is equal to $2^{N_{sub}}$. For a large structure, the size of the hypothesis space easily becomes intractable and the computational cost is prohibitive. To overcome these difficulties, we focus on the

relative comparisons of posterior probabilities, and devise a branch-and-bound method to facilitate the search of the hypothesis space. In addition, a simplified modeling technique is employed for multistory frame analyses. The following subsections discuss these three issues.

2.2 Determination of the Most Probable Damage Event

When applying Equation (4) to calculate the posterior probability $P(H_j|\hat{\Psi}_{N_s})$, the only undefined term is $P(\hat{\Psi}_{N_s}|H_j)$. The prior probability of a hypothesis $P(H_j)$ is the prior information given by users and the probability of estimated modal data $P(\hat{\Psi}_{N_s})$ is simply a normalizing constant.

As shown in Equation (1), less than a unity value for θ_i reflects the stiffness decrease in the ith substructure. As noted earlier, when θ_i is less than a specified threshold $\theta_i^*(< 1)$, the ith substructure is defined as *damaged*. If we define $\Theta_{H_j}^1$ as a set of θ_i's corresponding to the damaged substructures in a hypothesis H_j and $\Theta_{H_j}^2$ as the rest of θ_i's, the conditional probability $P(\hat{\Psi}_{N_s}|H_j)$ can be interpreted as the probability of obtaining $\hat{\Psi}_{N_s}$, when θ_i's in $\Theta_{H_j}^1$ are less than or equal to their threshold θ_i^*'s and the remaining θ_i's stay within $\theta_i^* < \theta_i \leq 1$. Denoting $\Omega_{H_j}^*$ as the range of Θ_{H_j} such that $0 \leq \Theta_{H_j}^1 \leq \Theta_{H_j}^{1,*}$ and $\Theta_{H_j}^{2,*} < \Theta_{H_j}^2 \leq 1$, the conditional probability $P(\hat{\Psi}_{H_j}|H_j)$ becomes:

$$
\begin{aligned}
P(\hat{\Psi}_{N_s}|H_j) = P(\hat{\Psi}_{N_s}|\Theta_{H_j} < \Omega_{H_j}^*) &= \frac{P(\hat{\Psi}_{N_s}, \Theta_{H_j} < \Omega_{H_j}^*)}{P(\Theta_{H_j} < \Omega_{H_j}^*)} \\
&= \frac{P(\Theta_{H_j} < \Omega_{H_j}^*|\hat{\Psi}_{N_s})\, P(\hat{\Psi}_{N_s})}{P(\Theta_{H_j} < \Omega_{H_j}^*)} \\
&= \frac{P(\hat{\Psi}_{N_s})}{P(\Theta_{H_j} < \Omega_{H_j}^*)} \int_{\Theta_{H_j} < \Omega_{H_j}^*} f(\Theta_{H_j}|\hat{\Psi}_{N_s}) d\Theta_{H_j} \qquad (6)
\end{aligned}
$$

where $\Theta_{H_j}^{1,*}$ and $\Theta_{H_j}^{2,*}$ are the sets of damage thresholds for $\Theta_{H_j}^1$ and $\Theta_{H_j}^2$, respectively, and $f(\Theta_{H_j}|\hat{\Psi}_{N_s})$ is a conditional probability density function (PDF) of Θ_{H_j} given $\hat{\Psi}_{N_s}$. Furthermore, $\Theta_{H_j} < \Omega_{H_j}^*$ indicates that Θ_{H_j} are within the range of $\Omega_{H_j}^*$ such that $0 \leq \Theta_{H_j}^1 \leq \Theta_{H_j}^{1,*}$ and $\Theta_{H_j}^{2,*} < \Theta_{H_j}^2 \leq 1$.

If we define the most probable parameter values $\Theta_{H_j}^{max}$, given a hypothesis H_j, such that:

$$
f(\Theta_{H_j}^{max}|\hat{\Psi}_{N_s}) = \max_{\Theta_{H_j} < \Omega_{H_j}^*} f(\Theta_{H_j}|\hat{\Psi}_{N_s}) \qquad (7)
$$

then the upper bound of $P(\hat{\Psi}_{N_s}|H_j)$ in Equation (6) becomes:

$$
\begin{aligned}
P_U(\hat{\Psi}_{N_s}|H_j) &= \frac{P(\hat{\Psi}_{N_s})}{P(\Theta_{H_j} < \Omega_{H_j}^*)} \int_{\Theta_{H_j} < \Omega_{H_j}^*} f(\Theta_{H_j}^{max}|\hat{\Psi}_{N_s}) d\Theta_{H_j} \\
&= \frac{P(\hat{\Psi}_{N_s})}{P(\Theta_{H_j} < \Omega_{H_j}^*)}\, f(\Theta_{H_j}^{max}|\hat{\Psi}_{N_s}) \int_{\Theta_{H_j} < \Omega_{H_j}^*} 1\, d\Theta_{H_j} \qquad (8)
\end{aligned}
$$

For simplification, we assume if damage occurs, it could have any arbitrary amount with equal probability. That is, we assign a uniform probability density function to θ_i such that:

$$f(\theta_i) = \begin{cases} 1 & \text{if } 0 \leq \theta_i \leq 1 \\ 0 & \text{otherwise} \end{cases} \tag{9}$$

Furthermore, if θ_i's are assumed to be independent, the following two equations hold:

$$f(\Theta_{H_j}) = \prod_{\forall\ \theta_i \in \Theta_{H_j}} f(\theta_i) = 1 \tag{10}$$

$$\frac{1}{P(\Theta_{H_j} < \Omega^*_{H_j})} = \frac{1}{\int_{\Theta_{H_j} < \Omega^*_{H_j}} f(\Theta_{H_j}) d\Theta_{H_j}} = \frac{1}{\int_{\Theta_{H_j} < \Omega^*_{H_j}} 1\, d\Theta_{H_j}} \tag{11}$$

Substituting Equation (11) into Equation (8), $P_U(\hat{\Psi}_{N_s}|H_j)$ can be simplified as:

$$P_U(\hat{\Psi}_{N_s}|H_j) = f(\Theta^{max}_{H_j}|\hat{\Psi}_{N_s})\ P(\hat{\Psi}_{N_s}) \tag{12}$$

The next step is to compute the conditional PDF, $f(\Theta^{max}_{H_j}|\hat{\Psi}_{N_s})$. First, let's define a modal error $e(n, \Theta_{H_j})$ as:

$$e(n, \Theta_{H_j}) = \hat{\psi}(n) - \psi(\Theta_{H_j});\ n = 1, ..., N_s \tag{13}$$

where $\hat{\psi}(n)$ is defined in Equation (3). Given Θ_{H_j}, an analytical modal data set $\psi(\Theta_{H_j})$ is defined similar to Equation (3) and is obtained by solving an eigenvalue problem, $\mathbf{K}(\Theta_{H_j})\,\mathbf{v}_i(\Theta_{H_j}) = \omega_i^2(\Theta_{H_j})\mathbf{M}\,\mathbf{v}_i(\Theta_{H_j})$:

$$\psi(\Theta_{H_j}) = \left[\omega_1(\Theta_{H_j}), ..., \omega_{N_m}(\Theta_{H_j}), \mathbf{v}_1^T(\Theta_{H_j}), ..., \mathbf{v}_{N_m}^T(\Theta_{H_j})\right]^T \in \mathbf{R}^{N_t} \tag{14}$$

It should be noted that, for a modal vector $\mathbf{v}_i(\Theta_{H_j})$ in Equation (14), only the components associated with the measured DOFs are included.

The modal error reflects the discrepancy between the measured response of the structure and the response of the associated analytical model. Two types of uncertainties account for this discrepancy. The first type of uncertainty is the measurement uncertainty caused by the presence of noise during vibration tests. The noise specifically accounts for the difference between the unknown true response and the measured response of the structure. The second type of uncertainty arises from the assumptions and simplifications introduced in the modeling process. Thus, the modal error defined in Equation (13) can be divided into two parts:

$$e(n, \Theta_{H_j}) = e_N(n) + e_M(\Theta_{H_j}) \tag{15}$$

where $e_N(n)$ is the modal error caused by the measurement noise in the nth vibration data set and $e_M(\Theta_{H_j})$ is the modal error caused by the modeling error. Assuming that each

entry or component of $e_N(n)$ is a normal distribution with zero mean, the expectation on both sides of Equation (15) with respect to N_s data sets becomes:

$$\mathbf{E}[e(n, \Theta_{H_j})] = \mathbf{E}[e_N(n)] + \mathbf{E}[e_M(\Theta_{H_j})] = e_M(\Theta_{H_j}) \tag{16}$$

where $e_M(\Theta_{H_j})$ is assumed to be constant for all N_s data sets. That is, the modeling error is caused only by the inherent difference between the analytical model and the structure regardless of the noise existence.

It appears that $e_M(\Theta_{H_j})$ changes according to the damage locations and amount. However, when damage is not severe, the modeling error can be assumed not to change significantly. In other words, the modal error caused by the modeling error $e_M(\Theta_{H_j})$ can be assumed to be constant and be approximated by $e_M(\Theta_{H_o})$, which is the modal error caused by the modeling error in the healthy (undamaged) state of the structure:

$$e_M(\Theta_{H_j}) \cong e_M(\Theta_{H_o});\ \forall \Theta_{H_j} \tag{17}$$

where H_o is a null hypothesis that there is no damage in the structure and the θ values of the healthy structure are calibrated to have unity values before any damage occurs. From the definition of the modal error and Equation (16), $e_M(\Theta_{H_o})$ can be evaluated from the estimated and the analytical modal parameter sets:

$$e_M(\Theta_{H_o}) = \mathbf{E}[e(n, \Theta_{H_o})] = \mathbf{E}[\hat{\psi}^h(n)] - \mathbf{E}[\psi(\Theta_{H_o})] = \hat{\psi}^h_m - \psi(\Theta_{H_o}) \tag{18}$$

where the superscript h denotes the properties of the healthy structure. Since $\psi(\Theta_{H_j})$ is constant with respect to the N_s data sets, $\mathbf{E}[\psi(\Theta_{H_o})] = \psi(\Theta_{H_o})$. Furthermore, the sample mean $\hat{\psi}^h_m$ is used to approximate the expectation $\mathbf{E}[\hat{\psi}^h(n)]$. The ith component of $\hat{\psi}^h_m$ is calculated such that:

$$\mathbf{E}[\hat{\psi}^h_i(n)] \cong \hat{\psi}^h_{m,i} = \frac{1}{N^h_s} \sum_{n=1}^{N^h_s} \hat{\psi}^h_i(n) \tag{19}$$

where $i = 1, ..., N_t$ and N^h_s is the number of modal data sets before damage occurrence. As a result, $e_M(\Theta_{H_j})$ can be evaluated from the measured modal parameter set $\hat{\psi}^h(n)$ of the healthy structure and the modal parameter set $\psi(\Theta_{H_o})$ of the initial analytical model:

$$e_M(\Theta_{H_j}) \cong e_M(\Theta_{H_o}) = \hat{\psi}^h_m - \psi(\Theta_{H_o})\ ;\ \forall \Theta_{H_j} \tag{20}$$

From the results of Equations (16) and (17), the error $\{e_i(n, \Theta_{H_j}); n = 1, ..., N_s\}$ for each component becomes a multivariate normal distribution with mean $e_{M,i}(\Theta_{H_o})$ and variance σ_i. Variance σ_i can be evaluated from the observation of the estimated modal parameter sets. When a large number of experimental data sets are available, sample standard deviations (or variances) can be extracted from the data set. When modal data sets available are not sufficient to estimate the variances, we assign uniform coefficient of

variance (COV) to all modal parameters. Assuming that the components of the modal error $e(n, \Theta_{H_j})$ are independent, the conditional joint PDF of Θ_{H_j} becomes:

$$f(\Theta_{H_j}|\hat{\Psi}_{N_s}) = f(e(n,\Theta_{H_j})|\hat{\Psi}_{N_s}) = k \cdot exp\Big\{ - J(\hat{\Psi}_{N_s}, \Theta_{H_j})\Big\} \tag{21}$$

where $k = \frac{1}{[2\pi]^{\frac{N_s}{2}}} \frac{1}{\|\mathbf{C}_{\hat{\Psi}}\|^{\frac{1}{2}}}$ and $\|\mathbf{C}_{\hat{\Psi}}\| = det|diag[\sigma_1^2, ..., \sigma_{N_t}^2]| = \prod_{i=1}^{N_t} \sigma_i^2$. Furthermore, the error function $J(\hat{\Psi}_{N_s}, \Theta_{H_j})$ is:

$$J(\hat{\Psi}_{N_s}, \Theta_{H_j}) = \tag{22}$$
$$\frac{1}{2}\sum_{n=1}^{N_s}[\hat{\psi}(n) - \psi(\Theta_{H_j}) - e_M(\Theta_{H_o})]^T \mathbf{C}_{\hat{\Psi}}^{-1}[\hat{\psi}(n) - \psi(\Theta_{H_j}) - e_M(\Theta_{H_o})]$$

From Equations (4), (12) and (21), the upper bound of $P(H_j|\hat{\Psi}_{N_s})$ becomes:

$$P_U(H_j|\hat{\Psi}_{N_s}) = f(\Theta_{H_j}^{max}|\hat{\Psi}_{N_s})P(H_j) = exp\Big\{ - J(\hat{\Psi}_{N_s}, \Theta_{H_j}^{max})\Big\} \cdot P(H_j) \cdot k \tag{23}$$

From Equation (23) and the fact that the relative comparison of $P_U(H_j|\hat{\Psi}_{N_s})$ is independent of the constant k, the following relationships hold:

$$\begin{aligned}\max\Big[P_U(H_i|\hat{\Psi}_{N_s}), P_U(H_j|\hat{\Psi}_{N_s})\Big] &= \max\Big[ln\, P_U(H_i|\hat{\Psi}_{N_s}), ln\, P_U(H_j|\hat{\Psi}_{N_s})\Big] \\ &= \min\Big[J(\hat{\Psi}_{N_s}, \Theta_{H_i}^{max}) - lnP(H_i), J(\hat{\Psi}_{N_s}, \Theta_{H_j}^{max}) - lnP(H_j)\Big]\end{aligned} \tag{24}$$

where ln denotes natural log. Therefore, the most probable hypothesis H_{max} in Equation (5) satisfies:

$$J(\hat{\Psi}_{N_s}, \Theta_{H_{max}}^{max}) - lnP(H_{max}) = \min_{\forall H_j}\Big[J(\hat{\Psi}_{N_s}, \Theta_{H_j}^{max}) - lnP(H_j)\Big] \tag{25}$$

Now, the comparison of posterior probabilities can be conducted by examining only the error function $J(\hat{\Psi}_{N_s}, \Theta_{H_j}^{max})$ and the prior probability $P(H_j)$. It should be noted that $P_U(H_j|\hat{\Psi}_{N_s})$ is employed rather than $P(H_j|\hat{\Psi}_{N_s})$ in Equation (24). The use of $P_U(H_j|\hat{\Psi}_{N_s})$ can be justified as follows: First, assume that H_d and $\Theta_{H_d}^{max}$ correspond to the actual damage locations and amount. In addition, noise effect is ignored for the current argument. Then, we can expect an inequality $f(\Theta_{H_d}^{max}|\hat{\Psi}_{N_s}) \geq f(\Theta_{H_j}|\hat{\Psi}_{N_s})$ for any H_j and Θ_{H_j}. That is, the conditional PDF of observing H_d and $\Theta_{H_d}^{max}$ is expected to be higher than or equal to any other damage cases (the equality holds when $H_j = H_d$ and $\Theta_{H_j} = \Theta_{H_d}^{max}$). From this observation and the fact that $P_U(H_j|\hat{\Psi}_{N_s}) = \int_{\Theta_{H_j} < \Omega_{H_j}^*} f(\Theta_{H_j}^{max}|\hat{\Psi}_{N_s}) d\Theta_{H_j}$, $P_U(H_d|\hat{\Psi}_{N_s}) \geq P_U(H_j|\hat{\Psi}_{N_s})$ holds for all H_j. However, if Θ_{H_d} differs from $\Theta_{H_d}^{max}$, the conditional PDF $f(\Theta_{H_d}|\hat{\Psi}_{N_s})$ can be less than other conditional PDFs even though H_d

corresponds to the actual damage locations. In other words, the PDF of *correct* damage locations and *incorrect* damage amount can be lower than PDFs of some other damage cases ($f(\Theta_{H_d}|\hat{\Psi}_{N_s}) < f(\Theta_{H_j}|\hat{\Psi}_{N_s})$ for some H_j and Θ_{H_j}). Consequently, $P(H_d|\hat{\Psi}_{N_s})$ can be less than $P(H_j|\hat{\Psi}_{N_s})$ for some H_j. In this case, we may fail to identify the actual damage event. Therefore, the use of $P_U(\hat{\Psi}_{N_s}|H_d)$ appears to increase the chance of identifying the actual damage locations and amount.

For given modal data, while we are interested in the probability $P_U(H_j|\hat{\Psi}_{N_s})$ of the assumed damage locations, the approach in Reference [3] calculates the conditional PDF $f(\Theta|\hat{\Psi}_{N_s})$ where $\Theta = \{\theta_1, ..., \theta_{N_{sub}}\}$, and θ_i is defined as a continuous variable with states ranging from 0 to 1. To obtain the probability for some parameter set Θ, a multi-dimensional integration for a desired Θ space is required. This multi-dimensional integral may not be feasible for a large scale model. This problem can be simplified by assuming that damage is localized in only a single substructure [3]. As an alternative, an asymptotic approach is proposed in Reference [2]. However, the asymptotic approach requires the calculation of all the maxima of $f(\Theta|\hat{\Psi}_{N_s})$, which is also a computationally expensive task.

In this study, we define the state of a substructure as *damaged* or *undamaged*. The binary states make it possible to construct a tree representation of all possible damage cases. The *damage tree* starts with a null hypothesis H_o that no damage is present. From the root, the first level branches are extended by adding a substructure as damaged one at a time. For a system with N_{sub} substructures, the number of the first level branches becomes ${}_{N_{sub}}C_1$. Here, we define ${}_NC_K (= \frac{N!}{K!(N-K)!})$ as the number of combinations of K items out of a population N. From each first level branch, the second level branches are extended by adding another substructure as damaged. The total number of the second level branches becomes ${}_{N_{sub}}C_2$. For a system with N_{sub} substructures, the damage tree has a total N_{sub} levels of branches and the total number of branches is $2^{N_{sub}} = {}_{N_{sub}}C_0 + {}_{N_{sub}}C_1 + ... + {}_{N_{sub}}C_{N_{sub}}$. Clearly, the number of alternatives remains large. The complexity can be significantly reduced by a branch-and-bound search scheme, which is originally proposed for the diagnosis of multiple diseases [12].

2.3 A Branch-and-Bound Search Scheme

A branch-and-bound search scheme is proposed to expedite the search for the most likely damage case without exhaustively examining all the possible combinations of damaged substructures. Starting from the null hypothesis H_0 that no damage is present, one substructure is added as a possible damage location at a time to generate extended hypotheses. The posterior probabilities of hypotheses are examined in terms of their error functions and the prior probabilities as defined in Equation (25). Each hypothesis keeps extending by adding a new substructure as damaged until the further addition of substructures does not lead to a more probable hypothesis. The key requirement is a bounding heuristic which allows us to rule out further extensions of a hypothesis. In this study, the following two pruning heuristics are adopted.

1. Let $H_j \cup D_i$ denote an extension of hypothesis H_j by adding the ith substructure as damaged. If a posterior probability of $H_j \cup D_i$ is less than that of H_j, then further

extension of $H_j \cup D_i$ is ruled out; i.e.

$$\text{if } P(H_j \cup D_i|\hat{\Psi}_{N_s}) < P(H_j|\hat{\Psi}_{N_s}), \text{ stop extending } H_j \cup D_i. \tag{26}$$

2. If a posterior probability of H_j is less than P_{max}, which is the largest posterior probability among all the hypotheses examined so far, then further extension of H_j is ruled out; i.e.

$$\text{if } P(H_j|\hat{\Psi}_{N_s}) < P_{max}, \text{ stop extending } \ H_j. \tag{27}$$

Using Equation (26), we can exclude the extension of $H_j \cup D_i$ when the addition of the ith substructure as damaged is found not to lead to a more probable hypothesis. In addition, when the first H_j is found such that $P(H_j|\hat{\Psi}_{N_s}) > P(H_j \cup D_i|\hat{\Psi}_{N_s})$ for all substructures not included in H_j ($\forall D_i \notin H_j$), $P(H_j|\hat{\Psi}_{N_s})$ is the first local maximum posterior probability in the current branching direction of damage events. That is, the criterion in Equation (26) guarantees that the first local maximum posterior probability in every branching direction is found. Unfortunately this pruning heuristic is not a strong criterion for the system with a large number of substructures since all branches are subject to further extensions until the first local maximum point is found.

As a complementary criterion, Equation (27) excludes the further branching of the newly extended hypotheses which have posterior probabilities less than the largest posterior probability among the hypotheses examined so far. The second criterion can be easily modified to include n number of the newly extended hypotheses for the further branching by replacing P_{max} in Equation (27) with the nth largest posterior probability P^n_{max}. By using the nth largest posterior probability, we can make an explicit trade-off between the better diagnosis and the computational efficiency.

2.4 Modeling of Multistory Frame Structures

The modeling of a multistory frame structure can be simplified by assuming that (1) the floor diaphragm is rigid in its own plane and only flexible in the vertical direction, (2) the rotational and vertical DOFs can be condensed out of the dynamic analysis, and (3) the axial deformations of beams and columns are negligible [7]. The system stiffness matrix of a multistory frame structure is determined from the lateral stiffness matrices of individual planar frames. The modeling process can be summarized as follows:

1. The stiffness matrix of each planar frame is first computed. Using the same notation as in Equation (1), the stiffness matrix of a frame j can be written as:

$$\mathbf{K}(\Theta)_j = \sum_{\forall i \in j} \theta_i \mathbf{K}_{si} \tag{28}$$

where the assembly is performed for each substructure i in the jth planar frame ($\forall i \in j$). Neglecting axial deformations in the columns and beams, the model of a planar frame has one in-plane rotational DOF at each node and one lateral DOF at each floor level [see Figure 1 (a)].

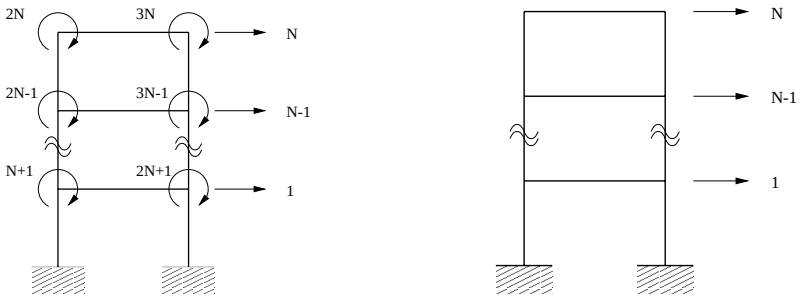

(a) Complete DOFs (b) Reduced DOFs

Figure 1: Calculation of Lateral Stiffness by Condensing out Rotational DOFs

2. The lateral stiffness matrix of the individual planar frame is determined from the stiffness matrix of the planar frame. The stiffness matrix of the planar frame can be partitioned according to the lateral (l) and rotational (r) DOFs, respectively:

$$\mathbf{K}(\Theta)_j = \begin{bmatrix} \mathbf{K}_{ll,j} & \mathbf{K}_{lr,j} \\ \mathbf{K}_{rl,j} & \mathbf{K}_{rr,j} \end{bmatrix} \tag{29}$$

Since the inertial effects associated with the rotational DOFs are usually small, the rotational DOFs can be condensed out of the dynamic analysis of the structure [see Figure 1 (b)]. Using static condensation, the lateral stiffness of the planar frame $\bar{\mathbf{K}}(\theta)_j$ becomes:

$$\bar{\mathbf{K}}(\Theta)_j = \mathbf{P}(\Theta)_j^T \, \mathbf{K}(\Theta)_j \, \mathbf{P}(\Theta)_j \tag{30}$$

where

$$\mathbf{P}(\Theta)_j = \begin{bmatrix} \mathbf{I} \\ -\mathbf{K}_{rr,j}^{-1} \, \mathbf{K}_{rl,j} \end{bmatrix} \tag{31}$$

and $\mathbf{I}$ is an identity matrix. It should be noted that the transformation matrix $\mathbf{P}(\Theta)_j$ is expressed as a function of Θ.

3. Using compatibility conditions, the displacement transformation matrix $\mathbf{G}_j$ can be defined to relate the lateral displacements of the jth frame to the global DOFs of the system:

$$\mathbf{u}_j = \mathbf{G}_j \mathbf{u}; \; j = 1, ..., N_f \tag{32}$$

where N_f is the number of planar frames, $\mathbf{u}$ are the global DOFs and $\mathbf{u}_j$ are the lateral DOFs of the jth planar frame. Figure 2 (a) shows the global DOFs of the system and the lateral DOFs of planar frames in the ith floor of a multistory system. An example of the displacement transformation matrix is shown in Figure 2 (b).

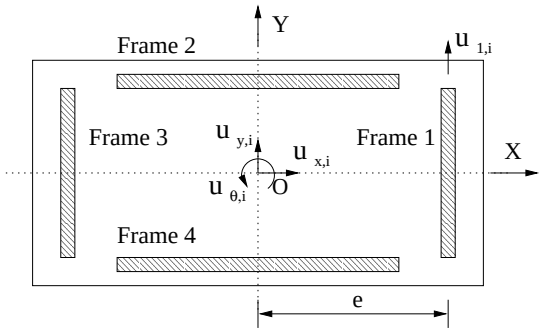

(a) the ith floor plan

$$\mathbf{u}_1 = \mathbf{G}_1 \begin{Bmatrix} \mathbf{u}_x \\ \mathbf{u}_y \\ \mathbf{u}_\theta \end{Bmatrix}$$

where

$$\mathbf{G}_1 = \begin{bmatrix} \mathbf{0} & \mathbf{I} & \mathbf{eI} \end{bmatrix}$$

(b) displacement transformation

Figure 2: Global DOFs of a System and Lateral DOFs of Planar Frames

4. Finally the system stiffness matrix of the simplified model is obtained by assembling the transformed stiffness matrices of all the planar frames:

$$\begin{aligned} \mathbf{K}(\Theta) &= \sum_{j=1}^{N_f} \mathbf{G}_j^T \bar{\mathbf{K}}_j \mathbf{G}_j = \sum_{j=1}^{N_f} \mathbf{G}_j^T \mathbf{P}(\Theta)_j^T \mathbf{K}(\Theta)_j \mathbf{P}(\Theta)_j \mathbf{G}_j \\ &= \sum_{j=1}^{N_f} \mathbf{T}(\Theta)_j^T \mathbf{K}(\Theta)_j \mathbf{T}(\Theta)_j \end{aligned} \tag{33}$$

where $\mathbf{T}(\Theta)_j$=$\mathbf{P}(\Theta)_j \mathbf{G}_j$. After substituting Equation (28) into Equation (33) and some manipulations, the stiffness matrix of the simplified model can be represented in a similar way to Equation (1):

$$\mathbf{K}(\Theta) = \sum_{j=1}^{N_f} \sum_{\forall i \in j} \theta_i \mathbf{T}(\Theta)_j^T \mathbf{K}_{si} \mathbf{T}(\Theta)_j = \sum_{i=1}^{N_{sub}} \theta_i \bar{\mathbf{K}}(\Theta)_{si} \tag{34}$$

where the effective stiffness contribution of the ith substructure is:

$$\bar{\mathbf{K}}(\Theta)_{si} = \sum_{\forall j \ni i} \mathbf{T}(\Theta)_j^T \mathbf{K}_{si} \mathbf{T}(\Theta)_j \tag{35}$$

To obtain the effective stiffness contribution of the ith substructure, the assembly is performed for all planar frames which include the ith substructure ($\forall j \ni i$). For example, when the ith substructure is common to planar frames 1 and 2, the stiffness contribution of the ith substructure to the system stiffness matrix is $\theta_i(\mathbf{T}(\Theta)_1^T \mathbf{K}_{si} \mathbf{T}(\Theta)_1 + \mathbf{T}(\Theta)_2^T \mathbf{K}_{si} \mathbf{T}(\Theta)_2)$.

This approach neglects compatibility of deformations in columns which are common to more than one frame. The assumption is acceptable except for tall slender buildings or tube type structures [1]. The system mass matrix is diagonalized by lumping the floor mass and the half masses of columns connected to the floor. The moment of inertia of the floor diaphragm is calculated about the vertical axis through the center of mass. Since the damage detection method requires repeated solution of the eigenvalue problem, the computational cost is significantly reduced by using the simplified model.

3 NUMERICAL EXAMPLES

This section presents three examples to illustrate the Bayesian probabilistic approach for the damage detection of frame structures. The example structures include a six story shear frame structure, and a two story and a five story three dimensional frame structure. For all examples, a uniform prior probability is assigned to all hypotheses. Therefore, the determination of the most probable hypothesis in Equation (25) depends only on the error function $J(\hat{\Psi}_{N_s}, \Theta_{H_j}^{max})$. For all numerical examples, the search space $\Theta_{H_j} < \Omega_{H_j}^*$ in Equation (7) is evaluated at the intersection of grid lines which discretizes the search domain with an incremental step $\Delta\theta$. For the presented numerical examples, we use an incremental step $\Delta\theta = 0.1$. In addition, a value of 0.9 is used for the damage threshold θ^* for every substructure. That is, over 10% decreases in the stiffness are defined as *damage*. Instead of the largest posterior probability P_{max}, we use the third largest posterior probability P_{max}^3 ($< P_{max}^2 < P_{max}^1 = P_{max}$) in Equation (27) to investigate a larger subspace of the hypothesis space. The branch-and-bound search in the presented examples follows a depth-first/best-first search strategy. Each modal vector is normalized with respect to the absolute maximum component in the modal vector. Since one component is used for normalization, only $N_d - 1$ pieces of information exist for each mode. For the examples shown below, L_{dam} and D_{dam} denote the actual damage locations and the associated damage amount, respectively. $\hat{L}_{dam}$ and $\hat{D}_{dam}$ denote the most probable damage locations and the associated damage amount estimated by the proposed method. In addition, the measured DOFs and the estimated modes are denoted by DOFm and MODEm, respectively.

3.1 A Six Story Shear Frame Structure

The first example structure is the six story shear frame structure shown in Figure 3. The frame structure consists of six DOFs and six substructures corresponding to each floor story. To simulate measurement uncertainties in the estimated modal parameters, the exact modal parameters, obtained from the analytical model with the assumed damage, are perturbed with noise. More explicitly, the estimated modal parameter set $\hat{\psi}(n)$

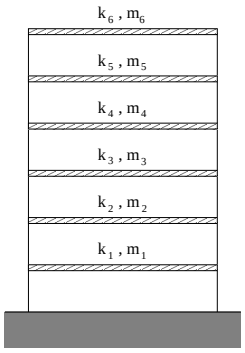

Figure 3: A Six Story Shear Frame Model

in Equation (3) is constructed such that:

$$\hat{\psi}(n) = \psi \ (1 + \frac{\mathcal{N}}{100} \ \mathcal{R}) \tag{36}$$

where ψ is the exact modal parameter set obtained from the analytical model, $\mathcal{N}$ is a specified noise level in terms of percentage, and $\mathcal{R}$ is a normally distributed random number with zero mean and a variance of 1.0. This process is repeated N_s times to simulate the N_s modal data sets.

Since the estimated modal parameters are simulated by adding noise to the exact modal parameters, the modal error defined in Equation (15) arises only from noise error, i.e. $e(n, \Theta_{H_j}) = e_N(n, \Theta_{H_j})$. Therefore the error function shown in Equation (22) is simplified as:

$$J(\hat{\Psi}_{N_s}, \Theta_{H_j}) = \frac{1}{2} \sum_{n=1}^{N_s} [\hat{\psi}(n) - \psi(\Theta_{H_j})]^T \mathbf{C}_{\hat{\Psi}}^{-1} [\hat{\psi}(n) - \psi(\Theta_{H_j})] \tag{37}$$

This example investigates the applicability of the proposed method subject to the effects of (1) the noise level in the estimated modal data, (2) the number and the selection of estimated modes and measured DOFs, (3) the locations and the amount of damage, and (4) the number of modal data sets.

3.1.1 Effect of Noise Level in the Estimated Modal Data

The proposed method is first tested to show that it does not give a false-positive indication of damage (the case of indicating damage when in fact damage does not exist). There cases are conducted assuming 3%, 5% and 10% noise levels. For each case, 10 sets of modal parameters are simulated from the *undamaged* structure, the DOFs corresponding to the second and fourth stories are measured, and the first and the second modes are identified. For all cases, the proposed method does not provide a false-positive indication.

Next, the effect of noise in the measured data is investigated. Four cases are conducted by varying the noise levels from 0.5% to 10%. For all cases, the stiffnesses of the second and the sixth stories are decreased by 30% and 10%, respectively, i.e. $L_{dam} = \{2, \ 6\}$ and $D_{dam} = \{30\%, \ 10\%\}$. The measurements are made at the second and the fourth stories, and the first and the second modes are identified, i.e. DOFm=$\{2, 4\}$ and MODEm=$\{1, 2\}$. Three sets of modal parameters are collected (N_s=3). Table 1 summarizes the results. The *rank* in the table indicates the rank of the actual damage event when the posterior probabilities of all examined hypotheses are sorted in descending order. As the noise level increases from case 1 to cases 2, 3 and 4, the rank of the actual damage event decreases.

3.1.2 Effect of Measured DOFs

The effect of measured DOFs is examined by changing the number and locations of the measured DOFs. Five cases are conducted by assuming $L_{dam} = \{2, \ 6\}$, $D_{dam} = \{30\%, \ 10\%\}$, $N_s = 5$ and a 10% noise level for the estimated modal parameters. Table 2 shows the results. When the modal vectors are obtained from the measurements on all

Table 1: Effect of Noise Level

Case	Noise level	Rank
1	0.5%	1
2	1.0%	5
3	5.0%	8
4	10.0%	10

L_{dam}={2,6}, D_{dam}={30%,10%}, N_s=3
Measured DOFs={2,4}, Estimated Modes={1,2}

DOFs (case 1) or on alternative floors (case 2), the proposed method correctly identifies the damage locations even in the presence of a 10% noise. As the number of measured DOFs decreases to two or one (cases 3, 4 and 5), the proposed method fails to rank the actual damage event as the most likely one. In case 5 of Table 2 (where only one DOF is measured), the proposed method uses only the estimated frequency information. No information is provided from modal vectors since the normalization of modal vectors requires the measurements of more than two DOFs. If a larger number of modal data sets were available, the diagnosis result could be improved. This is true even for the cases where only a limited number of locations are measured, and the data have relatively high noise level (see subsection 3.1.6).

Table 2: Effect of Measured DOFs

Case	DOFm	Rank
1	all	1
2	1,3,5	1
3	3,5	15
4	2,4	14
5	3	13

L_{dam}={2,6}, D_{dam}={30%,10%}, N_s=5
Estimated Modes={1,2}, Noise=10%

3.1.3 Effect of Multiple Damage Locations

One salient feature of this work is that multiple damage locations in a structure can be detected. As noted earlier, a branch-and-bound search scheme is employed to facilitate the search of multiple damage locations. Figure 4 presents a typical result of the branch-and-bound search. In this Figure, 10%, 20% and 30% damages are assumed in the first, the third and the fifth stories, respectively (L_{dam}={1, 3, 5} and D_{dam} = {10%, 20%, 30%}). The first two modes are estimated by the measurements on the second and the fourth stories (DOFm=[2, 4] and MODEm=[1, 2]). In addition, 10 modal data sets are simulated by assuming a 5% noise level (N_s=10 and Noise=5%).

Figure 4 shows that the proposed method finds the actual damage locations after searching 39 hypotheses out of the 64 possible hypotheses. The first story is detected as damaged immediately in the first step of branching. Since the decrease of the first story stiffness has a significant effect on all modal parameters, the first story is easily

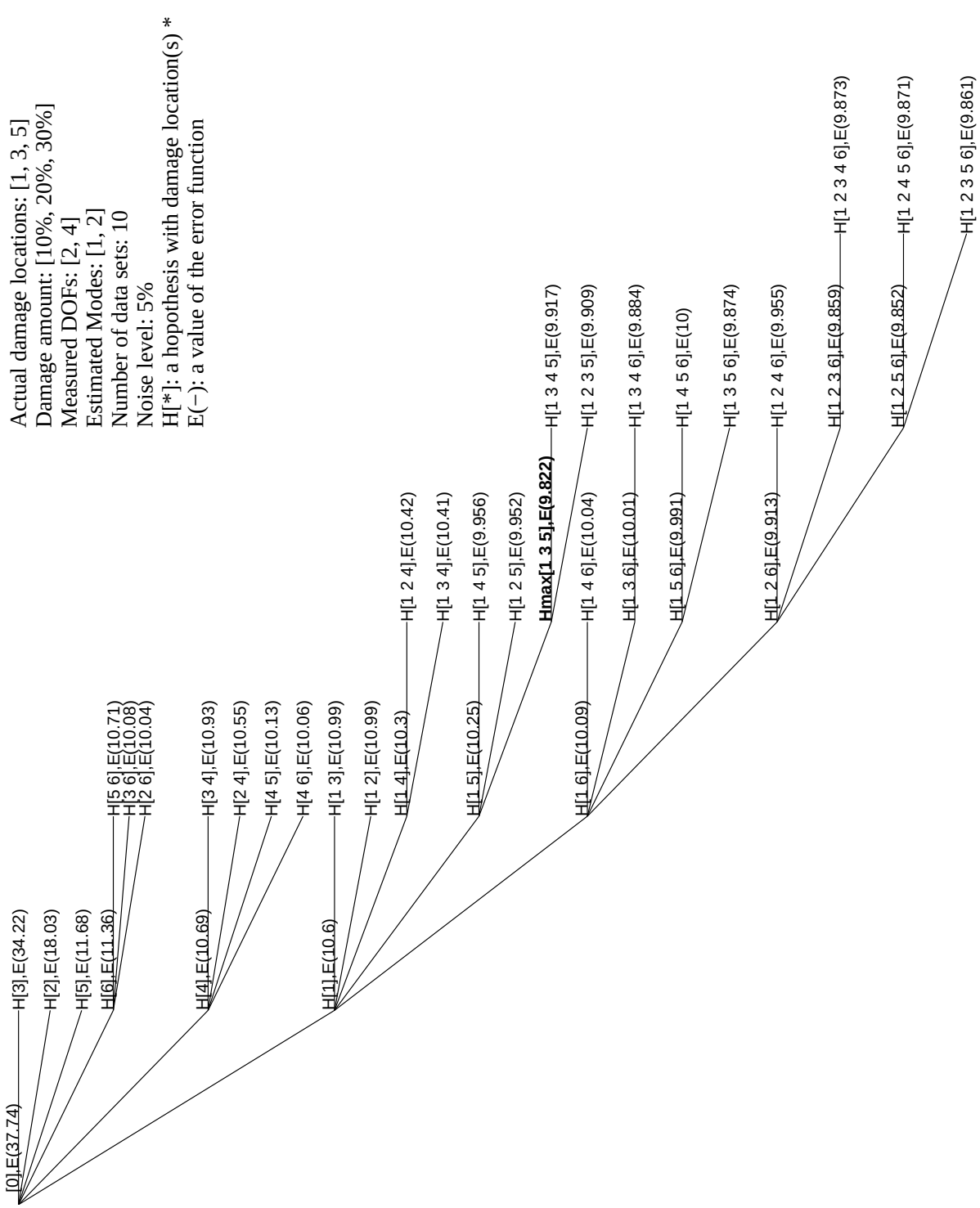

Figure 4: A Branch-and-Bound Search for Damage Locations of A Six Story Shear Frame Structure

detected as a damaged substructure. In the next step, the fifth story, which has the largest damage amount, is detected. Finally the third story is added as one of the possible damage locations. The correct damage hypothesis is extended one more step and bounded for further branching because the posterior probabilities of the extended hypotheses are lower than that of the correct hypothesis.

Figure 4 follows a depth-first/best-first search strategy. After the first extension of H[0] to H[1], H[4], H[6], H[5], H[2] and H[3], $P(\mathrm{H}[6]|\hat{\Psi}_{N_s})$ is assigned to P^3_{max}. Since the posterior probabilities of H[1], H[4] and H[6] are larger or equal to the current P^3_{max}, only these three branches remain for further extensions. Next, H[1] is extended since H[1] has the highest posterior probability among H[1], H[4] and H[6] (best-first search). After this extension, P^3_{max} is changed to $P(\mathrm{H}[1,4]|\hat{\Psi}_{N_s})$. Among the subtrees of H[1], only H[1,6], H[1,5] and H[1,4] remain for further extensions. In the next step, since we employ a depth-first search scheme, H[1,6] is first extended rather than H[4]. When we extend H[4] to H[4,6], H[4,5], H[2,4] and H[3,4], all branches below H[1] are already extended. That is, at this stage, P^3_{max} has been changed to $P(\mathrm{H}[1,2,5,6]|\hat{\Psi}_{N_s})$ which is the third largest posterior probability among the hypotheses examined so far. Since the posterior probabilities of H[4,6], H[4,5], H[2,4] and H[3,4] are less than the current P^3_{max}, further extensions are excluded.

In place of the largest posterior probability in Equation (27), Figure 4 uses the third largest posterior probability among the hypotheses examined so far as the pruning criterion. If the largest posterior probability had been used in Figure 4, the branching from hypothesis H(1) to H(1,5) would have been excluded. For the detection of multiple damage locations, the pruning heuristic in the branch-and-bound search scheme should be loosened to include a larger subspace of the hypothesis space. Examining more hypotheses increases the chance of capturing the actual damage event. In real situations, the proposed method may not find *all* the damaged substructures, but, very likely it can find the damage locations which have *significant* effect on the modal parameters.

3.1.4 Effect of Damage Amount

For all three cases in Table 3, we assume a 5% noise level, five sets of modal data, and the estimation of the first and the second modes with the measurement on the second and the fourth stories. The proposed method identifies the actual damage event for case 1, where 30% and 10% decreases in the stiffness are simulated in the second and the sixth stories, respectively. As damage in the second and the sixth stories respectively increases to 60% and 20% (case 2), the rank of the actual damage event decreases. When more severe damage is assumed for case 3 ($\hat{L}_{dam}$={2,6} and $\hat{D}_{dam}$={90%, 30%}), the rank of the actual damage event becomes lower. In spite of the absolute increase of damage in both the stories from case 1 to cases 2 and 3, the diagnosis result worsens. This phenomenon can be explained as follows: Since, in the current example structure, the second story stiffness has more significant effect on the modal parameters and larger damage than the sixth story stiffness, the second story becomes more detectable than the sixth story (for all cases, the branch-and-bound search identifies the second story first). On the other hand, the sixth story becomes less detectable as the difference of damage between the second and the sixth stories increases. This implies that, for the detection

Table 3: Effect of Damage Amount

Case	Damage Amount 2nd story	6th story	Rank
1	30%	10%	1
2	60%	20%	21
3	90%	30%	28

Measured DOFs={2,4}, N_s=5
Estimated Modes={1,2}, Noise=5%

of multiple damage locations, the proposed method depends on the *relative* damage amount among the damaged substructures as well as the *absolute* damage amount of each substructure. The cases shown in Table 3 use a value of 0.9 as the damage threshold value θ^* for all substructures. That is, the damaged substructures with less than 10% stiffness decrease may not be detected. If a higher damage threshold value (> 0.9) and a smaller $\Delta\theta$, which is an incremental value implemented to search the nondimensional parameter space $\Theta_{H_j} < \Theta^*_{H_j}$ in Equation (7), are used, the proposed method can identify smaller damage. For the cases shown in Table 4, we set the damage threshold value θ^* to 0.99 and the incremental value $\Delta\theta$ to 0.01. Four cases are conducted by changing the damage locations and amount. For all cases, less than 10% stiffness decrease is assumed. In spite of a small damage amount, all cases converge to the actual damage event. The problem is that the smaller the incremental value $\Delta\theta$, the more the computation time is required. Also the measured data with lower noise level is necessary for the detection of small damage.

3.1.5 Effect of Mode Selection

To study the effect of mode selection, the estimated modes are changed for each case. For all cases, the damage amount of the second and the sixth stories is assumed to be 30% and 10% respectively. Three modal data sets are collected and a 5% noise level is assumed. Measurements are made on the second and the fourth stories.

Table 5 presents the diagnosis results obtained by using four different mode selection strategies. When all six modes are estimated in case 1, the proposed method ranks the actual damage event as the most probable one. From the results of cases 2, 3 and 4, where two different modes are estimated for each case, it appears that the selection of the third and the fourth modes yields better assessment than the other two selection strategies for the detection of the assumed damage locations L_{dam}={2, 6}.

Table 4: Detection of Small Damage

Case	L_{dam}	D_{dam}	Noise	N_s	Rank
1	{3}	{3%}	2%	20	1
2	{1,3}	{5%,5%}	2%	100	1
3	{2,6}	{5%,3%}	5%	100	1
4	{2,3}	{5%,3%}	5%	50	1

Measured DOFs={2,4}, Estimated Modes={1,2}

Table 5: Effect of Mode Selection

Case	Estimated Modes	Rank
1	all	1
2	1, 2	8
3	3, 4	1
4	5, 6	7

L_{dam}={2,6}, D_{dam}={30%,10%}, N_s=3
Measured DOFs={2,4}, Noise=5%

What modes should be selected depends on the specified damage locations. Unfortunately, for the damage detection of civil structures, selecting specific modes may not be practical because (1) usually only a few fundamental modes can be estimated from the vibration test of a structure, and (2) the contribution of a mode for the damage detection depends on the actual damage locations which are unknown when modes are selected.

3.1.6 Effect of the Number of Modal Data Sets

Better damage assessment can be achieved by accumulating modal data sets from vibration tests. To investigate the effect of the number of modal data sets N_s, four cases are conducted by increasing N_s from 1 to 10. For all cases, $L_{dam} = \{2,\ 6\}$, $D_{dam} = \{30\%,\ 10\%\}$ and a 5% noise level are assumed. The first and the second modes are estimated by the measurements on the second and the fourth stories. The diagnosis results presented in Table 6 show that the proposed method identifies the actual damage locations when $N_s \geq 5$. For case 1, since the branch-and-bound search dose not find the actual damage event, the rank of the actual damage event is denoted as *not found* in Table 6.

Table 6: Effect of Data Set Number

Case	N_s	Rank
1	1	not found
2	3	8
3	5	1
4	10	1

L_{dam}={2,6}, D_{dam}={30%,10%}, Noise=5%
Measured DOFs={2,4}, Estimated Modes={1,2}

Table 7 shows the results of the re-diagnosis of the previous cases, which failed to rank the actual damage event as the most probable one, by increasing the number of data sets. For the previous case 3 of Table 1, the rank of the actual damage event changes from eighth to first after increasing the number of data sets N_s from 3 to 5. Table 7 also shows the other cases in which the actual damage locations are properly detected after increasing N_s. However, for the previous case 5 of Table 2, where only one DOF is measured, the proposed method fails to identify the actual damage locations even after increasing N_s to 20. This illustrates that sufficient measured DOFs and number of data sets are required for damage detection.

Table 7: Improvement of Diagnosis Results by Increasing Data Set Number

Case	D_{dam}	Noise	MODEm	DOFm	N_s	Rank
case 2 of table 1	{30%,10%}	1%	{1,2}	{2,4}	3→5	5→1
case 3 of table 1	{30%,10%}	5%	{1,2}	{2,4}	3→5	8→1
case 4 of table 1	{30%,10%}	10%	{1,2}	{2,4}	3→20	10→1
case 2 of table 3	{60%,20%}	5%	{1,2}	{2,4}	5→10	21→1
case 3 of table 3	{90%,30%}	5%	{1,2}	{2,4}	5→10	28→1
case 4 of table 5	{30%,10%}	5%	{5,6}	{2,4}	3→20	7→1
case 3 of table 2	{30%,10%}	10%	{1,2}	{3,5}	5→20	15→1
case 4 of table 2	{30%,10%}	10%	{1,2}	{2,4}	5→20	14→1
case 5 of table 2	{30%,10%}	10%	{1,2}	{3}	5→20	13→9

For all cases, L_{dam}={2, 6}

3.2 A Two Story Three Dimensional Frame Structure

A two story frame structure, shown in Figure 5, is employed to validate the proposed method for three dimensional problems. The analytical model is assumed to be identical to the actual structure, and has 48 DOFs (24 rotational DOFs and 24 translational DOFs). Each beam and column is modeled as a substructure. Altogether, the system consists of 16 substructures. For all the cases considered in this example, five fundamental modes are estimated. The modal parameters are measured at 5 DOFs out of the total 48 DOFs. Two configurations of the measured DOFs are shown in Figure 6. In addition, three sets of the estimated modal parameters are simulated by perturbing the exact modal parameters with a 5% noise level.

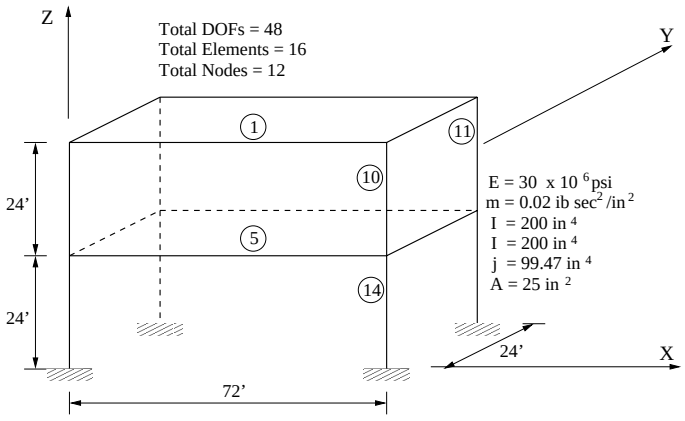

Figure 5: A Two Story Frame Structure

As shown in Table 8, the four cases are conducted by changing the damage locations and amount. The modal parameters are measured at the DOFs shown in Figure 6 (a). For case 1, the first substructure is subject to a 20% decrease in the stiffness. Case 2 assumes 20% and 40% stiffness decreases in the 10th and the 11th substructures, respectively. Case 3 assumes 20% and 40% stiffness decreases in the 1st and the 14th substructures,

Table 8: Diagnosis Results of A Two Story Frame Structure

	Actual Damage		Estimated Damage			
Case	L_{dam}	D_{dam}	$\hat{L}_{dam}$	$\hat{D}_{dam}$	N_s	Rank
1	{1}	{20%}	{1}	{20%}	5	1
2	{10,11}	{20%,40%}	{10,11}	{20%,40%}	5	1
3	{1,14}	{20%,40%}	{1,11,14}	{20%,20%,40%}	5	1
			{1,14}	{20%,40%}		2
4	{1,14}	{20%,40%}	{1,14}	{20%,40%}	10	1

Measured DOFs={3,16,28,32,48}, Estimated Modes={1,2,3,4,5}
Noise=2%, N_s=5

Table 9: Comparison of Two Measurement Strategies

Case	DOFm	Rank
5	{3,16,28,32,48}	not found
6	{8,13,20,25,32}	1

Estimated Modes={1,2,3,4,5}, Noise=2%, N_s=5
L_{dam}={1,5}, D_{dam}={20%,40%}

respectively. All the damaged substructures are shown as circled numbers in Figure 5. For cases 1 and 2, the proposed method finds the exact damage locations as well as the exact damage amount. Case 3 ranks the actual damage event as the second most probable event; the most probable event corresponds to the actual damage locations (the 1st and the 14th substructures) with one extra location (the 11th substructure). After increasing the number of modal data sets from 5 to 10, the actual damage event is properly identified as the most likely one as shown in case 4.

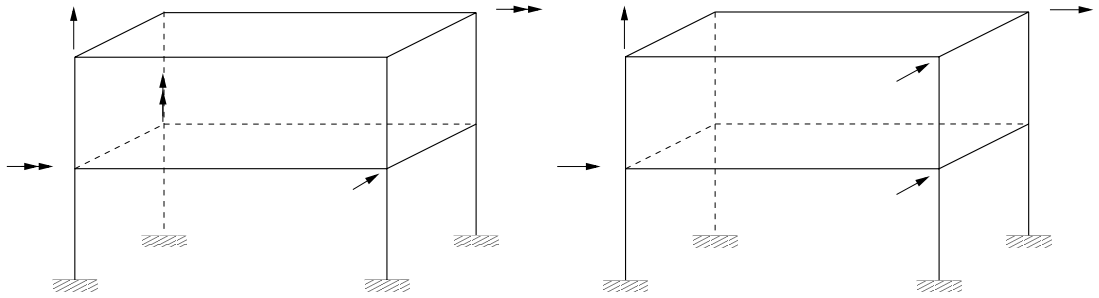

(a) measurement configuration 1
DOFm={3, 16, 28, 32, 48}

(b) measurement configuration 2
DOFm={8, 13, 20, 25, 32}

Figure 6: Two Different Configurations of Measured DOFs

Table 9 investigates the effect of measured DOFs on damage detection by comparing two different configurations of measured DOFs as shown in Figure 6. 20% and 40% damage are assumed in the first and the fifth substructures for both cases. Since the actual damage event is not found by the branch-and-bound search for case 5, the rank

of the actual damage event is represented as *not found* in Table 9. In dynamic analyses, the inertial effects associated with rotational DOFs are usually small. In addition, the axial deformations of beams and columns can be ignored in many cases. As a result, lateral DOFs provide more information than rotational and vertical DOFs. For case 5, three rotational, one vertical and one horizontal DOFs (DOFm={3, 16, 28, 32, 48}) are measured, and for case 6 the measured DOFs {8, 13, 20, 25, 32} are all lateral DOFs. The results of Table 9 show that the measured DOFs in case 6 are more appropriate for the detection of damage in the first and the fifth substructures.

3.3 A Five Story Three Dimensional Frame Structure

The applicability of the proposed method is illustrated when differences exist between the baseline structure and the simplified model. The first example neglects the measurement noise to highlight the effect of modeling error, and the second example considers both modeling and noise errors. In this example, a FE model of a five story frame structure serves as the baseline structure. The term *baseline structure* is used to represent a structure from which the experimental modal parameters are simulated. A simplified model, which the proposed method works with, is formed by employing the modeling approach described in Subsection 2.4. Furthermore, for the calculation of $e_M(\Theta_{H_o})$ in Equation (18), $\hat{\psi}_m^h$ is simulated by perturbing the modal parameters of the initial FE model with noise. $\psi(\Theta_{H_o})$ is obtained by solving an eigenvalue problem of the simplified model. That is, $e_M(\Theta_{H_o})$ is defined as the modal error caused by the difference between the baseline structure and the simplified model.

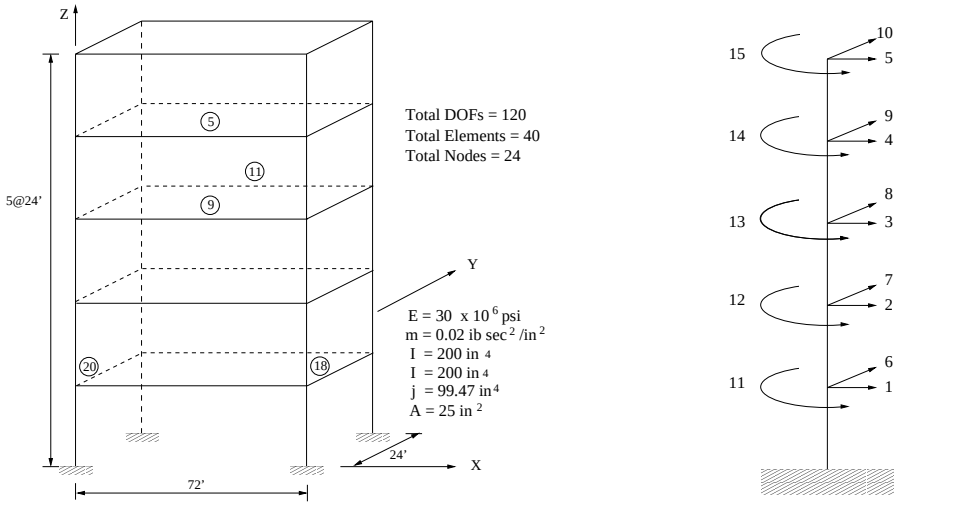

(a) the baseline structure (b) the simplified model

Figure 7: The Baseline Structure and The Simplified Model of A Five Story Frame Structure

Figure 7 (a) and (b) show the baseline structure and the simplified model, respectively. While the baseline structure has 6 DOFs at each node (three translational and three rotational DOFs), the simplified model has only 3 DOFs at the mass center of each floor. For the current five story example, the baseline structure has 120 DOFs and the simplified

Table 10: Effect of Modeling Error in A Five Story Frame Structure

	Actual Damage		Estimated Damage		
case	L_{dam}	D_{dam}	$\hat{L}_{dam}$	$\hat{D}_{dam}$	N_s
1	{5,9}	{50%,50%}	{5,9}	{60%,50%}	1
2	{9,11}	{40%,60%}	{9,11}	{50%,70%}	1
3	{18,20}	{20%,10%}	{18,20}	{20%,10%}	1

Noise=0%, Measured DOFs={1,2,...,15}, Estimated Modes={1,2,...,6}

model has 15 DOFs. In many vibration tests of building structures, modal vectors are evaluated at the mass center of the floor diaphragm. To simulate the estimated modal vectors of a structure, the modal vector of the FE model is reconstructed at the mass center of every floor. That is, the components of the estimated modal vector correspond with those of the simplified model. The first six fundamental modes are assumed to be estimated. The first and fourth modes are the first and second bending modes, respectively, in the X-direction of Figure 7. The second and fifth modes are the first and second bending modes, respectively, in the Y-direction. Furthermore, the third and sixth modes correspond to the first and second torsional modes, respectively.

3.3.1 Consideration of Modeling Error

Table 10 shows the diagnosis results of three different damage scenarios, considering the difference between the baseline structure and the simplified model. Case 1 assumes a 50% stiffness decrease in the 5th and the 9th substructures. For case 2, 40% and 60% decreases in the stiffness are imposed on the 9th and the 11th substructures, respectively. Case 3 assumes 20% and 10% stiffness decreases in the 18th and the 20th substructures, respectively. Figure 7 (a) shows the damaged substructures as circled numbers. Substructures are defined as beams and columns in the baseline structure. Since the stiffness matrix of the simplified system is represented as an assembly of the effective stiffness contribution of each substructure [see Equation (34)], damage locations can be tracked at the substructure level of the baseline structure. That is, damage locations are identified in the baseline structure, not in the simplified model.

For all cases, the proposed method properly identifies the actual damage locations. The estimated damage amount is, however, slightly different from the actual damage amount for cases 1 and 2. This can be explained as follows: We search for the most likely hypothesis H_{max} and the corresponding nondimensional parameter value $\Theta_{H_{max}}^{max}$ which minimize the approximated error function $J(\hat{\Psi}_{N_s}, \Theta_{H_j})$ defined in Equation (22). For the exact definition of $J(\hat{\Psi}_{N_s}, \Theta_{H_j})$, $e_M(\Theta_{H_d})$, which is the modal error caused by the modeling error after damage occurrence, should be evaluated. However, the actual damage locations and amount, which are required to evaluate $e_M(\Theta_{H_d})$, are unknown. Therefore, $e_M(\Theta_{H_d})$ is approximated by $e_M(\Theta_{H_o})$, which is the modal error caused by the modeling error before damage occurrence, assuming that the modeling error is constant for arbitrary damage locations and amount ($e_M(\Theta_{H_j}) \cong e_M(\Theta_{H_o})$; $\forall \Theta_{H_j}$).

For comparison of $e_M(\Theta_{H_o})$ and $e_M(\Theta_{H_j})$, the selected components of $e_M(\Theta_{H_o})$ and $e_M(\Theta_{H_j})$ are listed in Table 11. The error components corresponding to the first six

Table 11: Comparison of $e_M(\Theta_{H_o})$ and $e_M(\Theta_{H_j})$

	$\psi_i(\Theta_{H_o})$	$e_{M,i}(\Theta_{H_o})$	$e_{M,i}(\Theta_{H_j})$		
			Case 1	Case 2	Case 3
		(a) Components corresponding to the frequencies			
Mode	ω_i				
1	1.7313	0.0030	0.0053 (0.13%)	0.0035 (0.02%)	0.0030 (0.00%)
2	2.4566	0.0281	0.0282 (0.00%)	0.0282 (0.00%)	0.0281 (0.00%)
3	2.9106	0.0070	0.0079 (0.03%)	0.0082 (0.04%)	0.0076 (0.02%)
4	5.7511	0.0157	0.0014 (0.30%)	0.0078 (0.14%)	0.0157 (0.00%)
5	7.6658	0.0935	0.0943 (0.01%)	0.0948 (0.02%)	0.0948 (0.02%)
6	9.1053	0.0956	0.0557 (0.44%)	0.0415 (0.59%)	0.0981 (0.03%)
		(b) Components corresponding to the modal vectors			
DOF	$\mathbf{v}_1$				
1	0.1559	0.0003	0.0002 (0.06%)	0.0002 (0.05%)	0.0003 (0.00%)
2	0.4274	0.0009	0.0004 (0.12%)	0.0006 (0.05%)	0.0009 (0.00%)
3	0.6865	0.0013	0.0001 (0.17%)	0.0011 (0.03%)	0.0013 (0.00%)
4	0.8822	0.0012	0.0007 (0.06%)	0.0011 (0.02%)	0.0012 (0.00%)
5	1.0000	0.0000	0.0000 (0.00%)	0.0000 (0.00%)	0.0000 (0.00%)
DOF	$\mathbf{v}_2$				
6	0.1998	0.0014	0.0014 (0.00%)	0.0014 (0.00%)	0.0015 (0.03%)
7	0.4834	0.0029	0.0029 (0.00%)	0.0029 (0.00%)	0.0031 (0.02%)
8	0.7312	0.0032	0.0032 (0.00%)	0.0032 (0.00%)	0.0033 (0.01%)
9	0.9077	0.0018	0.0018 (0.00%)	0.0018 (0.00%)	0.0019 (0.01%)
10	1.0000	0.0000	0.0000 (0.00%)	0.0000 (0.00%)	0.0000 (0.00%)
DOF	$\mathbf{v}_3$				
11	0.1987	0.0001	0.0002 (0.03%)	0.0002 (0.02%)	0.0002 (0.05%)
12	0.4849	0.0022	0.0019 (0.07%)	0.0018 (0.08%)	0.0020 (0.04%)
13	0.7345	0.0029	0.0027 (0.02%)	0.0031 (0.04%)	0.0029 (0.01%)
14	0.9102	0.0013	0.0016 (0.03%)	0.0019 (0.06%)	0.0014 (0.01%)
15	1.0000	0.0000	0.0000 (0.00%)	0.0000 (0.00%)	0.0000 (0.00%)
DOF	$\mathbf{v}_4$				
1	0.4996	0.0005	0.0006 (0.04%)	0.0005 (0.01%)	0.0005 (0.00%)
2	0.9619	0.0022	0.0011 (0.11%)	0.0002 (0.21%)	0.0022 (0.00%)
3	0.6984	0.0084	0.0059 (0.36%)	0.0071 (0.19%)	0.0084 (0.00%)
4	-0.1532	0.0119	0.0103 (1.05%)	0.0119 (0.01%)	0.0119 (0.00%)
5	-1.0000	0.0000	0.0000 (0.00%)	0.0000 (0.00%)	0.0000 (0.00%)
DOF	$\mathbf{v}_5$				
6	0.5963	0.0004	0.0003 (0.01%)	0.0003 (0.01%)	0.0013 (0.15%)
7	1.0000	0.0000	0.0000 (0.00%)	0.0000 (0.00%)	0.0000 (0.00%)
8	0.6238	0.0017	0.0016 (0.02%)	0.0016 (0.02%)	0.0024 (0.11%)
9	-0.2603	0.0020	0.0022 (0.06%)	0.0025 (0.18%)	0.0025 (0.17%)
10	-0.9869	0.0071	0.0069 (0.03%)	0.0062 (0.10%)	0.0070 (0.09%)
DOF	$\mathbf{v}_6$				
11	0.5824	0.0021	0.0180 (2.73%)	0.0319 (5.12%)	0.0038 (0.29%)
12	0.9756	0.0053	0.0447 (4.04%)	0.0748 (7.12%)	0.0015 (0.39%)
13	0.5881	0.0125	0.0529 (6.86%)	0.0855 (12.4%)	0.0095 (0.51%)
14	-0.2931	0.0164	0.0348 (6.30%)	0.0466 (10.3%)	0.0148 (0.54%)
15	-1.0000	0.0000	0.0000 (0.00%)	0.0000 (0.00%)	0.0000 (0.00%)

*The value in ( ) represents the normalized error, $100 \times |e_{M,i}(\Theta_{H_o}) - e_{M,i}(\Theta_{H_j})|/\psi_i(\Theta_{H_o})$, in percentage

Table 12: Effect of Modeling and Noise Errors in A Five Story Frame Structure

	Actual Damage		Estimated Damage		
case	L_{dam}	D_{dam}	$\hat{L}_{dam}$	$\hat{D}_{dam}$	N_s
1	{5,9}	{50%,50%}	{5,9}	{60%,50%}	5
2	{9,11}	{40%,60%}	{9,11}	{50%,70%}	10
3	{18,20}	{20%,10%}	{18,20}	{20%,10%}	10

Noise=5%, Measured DOFs={1,2,...,15}, Estimated Modes={1,2,...,6}

frequencies are shown in part (a) of Table 11. Next the error components corresponding to the measured modal vectors are presented in part (b). For simplicity, only the components corresponding to the DOFs 1 - 5 are tabulated for the first and fourth modal vectors (the first two bending modes along the X-direction). Similarly, the components corresponding to the DOFs 6 - 10 are presented for the second and fifth modal vectors (the first two bending modes along the Y-direction), and the components corresponding to the DOFs 11 - 15 are presented for the third and sixth modal vectors (the first two torsional modes). $e_M(\Theta_{H_j})$ is computed for the three damage cases in Table 10. To provide a relative measure on the magnitude of $e_M(\Theta_{H_o})$, the components of $\psi(\Theta_{H_o})$ corresponding to those of $e_M(\Theta_{H_o})$ are presented in the first column of each table. Furthermore, a normalized error defined as $100 \times |e_{M,i}(\Theta_{H_o}) - e_{M,i}(\Theta_{H_j})|/\psi_i(\Theta_{H_o})$ is parenthesized next to each $e_{M,i}(\Theta_{H_j})$ value.

For cases 1 and 2 of Table 11, larger differences between $e_M(\Theta_{H_j})$ and $e_M(\Theta_{H_o})$ than those of case 3 are observed especially in the components corresponding to mode 6. This explains why the estimated damage amount is slightly different from the actual damage amount for cases 1 and 2. It appears that $|e_{M,i}(\Theta_{H_o}) - e_{M,i}(\Theta_{H_j})|$ increases for higher modes. However, the magnitude of $|e_{M,i}(\Theta_{H_o}) - e_{M,i}(\Theta_{H_j})|$ remains less than 1 % of the corresponding $\psi_i(\Theta_{H_o})$ for most components. Since the damage amount is small in case 3, the change of the modeling error is negligible, and the proposed method identifies the exact damage amount as well as the correct damage locations. From this simplification, we are able to reduce the size of the system from 120 DOFs to 15 DOFs without losing significant accuracy.

3.3.2 Consideration of Modeling and Noise Errors

Finally, the measurement noise and the modeling error are taken into account together to validate the robustness of the proposed method. The same damage scenarios in Table 10 are re-investigated. The only difference from the previous cases is that the modal parameters of the FE model are corrupted with 5% noise. Table 12 summarizes the diagnosis results. After increasing the number of modal data sets to a certain number, the proposed method identifies the actual damage locations even in the presence of the measurement noise and the discrepancy between the baseline structure and the simplified model.

4 CONCLUSIONS AND DISCUSSION

In this paper, a Bayesian probabilistic approach has been applied to detect the most likely locations and amount of damage in a structure. The system stiffness matrix is represented

as an assembly of the substructure stiffness matrices and a nondimensional parameter θ_i is introduced to model the stiffness contribution of the ith substructure. The mass matrix is assumed to be known and invariant. Assuming a uniform probability density function for the nondimensional parameter θ_i ($0 \leq \theta_i \leq 1$), we formulate the relative posterior probability of an assumed damage event and apply a branch-and-bound search scheme to identify the most likely damage event. The measurement noise and modeling error between the structure and the analytical model are explicitly considered within the Bayesian probabilistic framework.

Several examples using a shear frame structure, a two story and a five story three dimensional frame structure are simulated to assess the potential applicability of the proposed method. As long as sufficient modal data sets are available, the proposed method is able to identify the actual damage locations and amount in most cases where (1) less than 10% noise levels are achieved in the estimated modal parameters, (2) only 10%-30% out of the total degrees of freedom are measured, and (3) only several fundamental modes are estimated. The computational cost of the method is significantly reduced by using a branch-and-bound search scheme.

While this paper has illustrated the potential applicability of the Bayesian probabilistic approach to damage detection, many interesting research issues remain. First, the computational effort to find the most likely nondimensional parameter value $\Theta_{H_j}^{max}$ in Equation (7), increases exponentially with the number of potentially damaged substructures included in the hypothesis H_j. The computation could become prohibitive when $\Theta_{H_j}^{max}$ is calculated for a hypothesis H_j which assumes a large number of substructures as damaged. Further effort is required to develop an efficient method to evaluate $\Theta_{H_j}^{max}$.

Second, damage detection techniques, which rely only on the modal parameter information such as the one described in this paper, might have the drawback that the damage locations and amount may not be uniquely determined from the estimated modal data [24]. Models with differently assumed damage locations and amount can produce identical modal parameters. These models are referred to as *output equivalent* models [18]. The exhaustive search of all possible models (hypotheses) is infeasible, and a branch-and-bound search scheme may identify only some models (hypotheses with assumed damage locations and amount), which locally maximize the posterior probability $P(H_j|\hat{\Psi}_{N_s})$ in Equation (5), and may not detect the global maximum points. In real applications, (1) since the modal testing measures the dynamic responses at limited points and estimates only a few fundamental modes, the number of output equivalent models can increase, and (2) in the presence of the modeling error and the measurement noise, some erroneous models could have modal parameters closer to the estimated modal parameters than the model with the correct damage locations and amount. Therefore, in practice, more hypotheses should be examined to find more local maximum posterior probabilities and potentially to identify the correct damage event. In the proposed method, a larger subspace of the hypothesis space can be examined by replacing P_{max} in Equation (27) with P_{max}^n, where P_{max}^n is the nth largest posterior probability among the hypotheses examined so far. This approach allows us to make an explicit trade-off between the computational cost and the better diagnosis. However further research is required to provide a systematic guideline for choosing "n" in P_{max}^n .

Third, damage is simulated as the deterioration of substructure or element stiffnesses in this paper. In real structures, damages are developed in the form of fatigue cracks, loose connections, local bucklings and so on. It is not clear if the substructure approach can capture these kinds of real damage within the substructure. Further study is required to relate the physical damage phenomena to the mathematical damage models.

The proposed method is superior to the deterministic approaches, which produce a single diagnosis result, in that (1) several suspicious damage events are provided with their relative possibilities, (2) a series of measurement data obtained from vibration tests can be included to improve the accuracy of the results, and (3) engineering judgment about possible damage events via some system reliability analysis or experience with similar structures can potentially be incorporated into the Bayesian framework as the prior probabilities of the damage events.

Acknowledgments

This research is partially sponsored by the National Science Foundations under Grant No. CMS-95261-2. Valuable discussions with Professor Anne S. Kiremidjian and Mr. Erik G. Straser at Stanford University and Professor James L. Beck at California Institute of Technology are sincerely appreciated. The comments by the reviewers are also appreciated.

References

1. A. K. Ahmadi, 'Application of system identification in mathematical modeling of buildings', *Ph.D. Thesis*, Department of Civil Engineering, University of Pittsburgh, Pittsburgh, PA, 1986.
2. J. L. Beck and L. S. Katafygiotis, 'Probabilistic system identification and health monitoring of structures', *Proc. 10th world conf. on earthquake engineering*, Balkema, Rotterdam, 1992.
3. J. L. Beck, M. W. Vanik, and L. S. Katafygiotis, 'Determination of stiffness changes from modal parameter changes for structural health monitoring', *Proc. 1st world conf. on structural control*, Pasadena, CA, 1994.
4. J. S. Bendat and A. G. Piersol, *Random Data: Analysis and Measurement procedures*, 2nd edn, Wiley, New Year, 1986.
5. A. Berman and E. J. Nagy, 'Improvements of a large analytical model using test data', *AIAA* **21**, 1168-1173 (1983).
6. J. C. Chen and J. A. Garba, 'On-orbit damage assessment for large space structures', *AIAA* **26**, 1119-1126 (1988).
7. A. K. Chopra, *Dynamics of Structures*, Prentice Hall, New Jersey, 1995.
8. C. R. Farrar *et al.* 'Dynamic characterization and damage detection in the I-40 bridge over the Rio Grande', *Report No. LA*-12767-*MS*, Los Alamos National Laboratory, Los Alamos, NM, 1994.
9. G. V. Garcia and N. Stubbs, 'Relative performance evaluation of pattern recognition models for nondestructive damage detection (NDD)', *Proc. 15th int. modal analysis conf.*, Orlando, FL, 1997.
10. J. He and D. J. Ewins, 'Compatibility of measured and predicted vibration modes in model improvement studies', *AIAA* **29**, 798-803 (1991).
11. F. M. Hemez, 'Theoretical and experimental correlation between finite element models and modal tests in the context of large flexible space structures', *Ph.D. thesis*, Department of Aerospace Engineering, University of Colorado at Boulder, Boulder, COL, 1993.

12. M. Henrion, 'Towards efficient probabilistic diagnosis in multiply connected belief networks', *Influence Diagrams, Belief Nets and Decision Analysis, chapter 17*, Wiley, Chichester, 1990.
13. M. Imregun and D. J. Ewins, 'An investigation into mode shape expansion techniques', *Proc. 11th int. modal analysis conf.*, Kissimmee, FL, 1993.
14. G. H. James, D. C. Zimmerman, C. R. Farrar, S. W. Doebling, 'Current horizon for structural damage detection course', *SEM short course held at the 15th int. modal analysis conf.*, Orlando, FL, 1997.
15. A. M. Kabe, 'Stiffness matrix adjustment using mode data', *AIAA* **23**, 1431-1436 (1985).
16. D. C. Kammer, 'Optimum approximation for residual stiffness in linear system identification', *AIAA* **26**, 104-112 (1988).
17. M. Kaouk and D.C. Zimmerman, 'Structural damage assessment using a generalized minimum rank perturbation theory', *Proc. 34th AIAA/ASME/ASCE/AHS structure, structural dynamics & material conf.*, La Jolla, CA, 1993.
18. L. S. Katafygiotis, 'Treatment of model uncertainties in structural dynamics', *EERL Report No.* 91-01, Earthquake Engineering Research Laboratory, California Institute of Technology, Pasadena, CA, 1991.
19. J. M. Ricles and J. B. Kosmatka, 'Damage detection in elastic structures using vibratory residual forces and weighted sensitivity', *AIAA* **30**, 2310-2316 (1992).
20. S. W. Smith, 'Damage detection and location in large space trusses', *Ph.D. Thesis*, Virginia Polytechnic Institute and State University, Blacksburg, VA, 1988.
21. S. W. Smith and C. A. Beattie, 'Simultaneous expansion and orthogonalization of measured modes for structure identification', *AIAA Report No.* 90-1218-*CP*, 1990.
22. S. W. Smith and C. A. Beattie, 'Secant-method adjustment for structural models', *AIAA* **29**, 119-126 (1991).
23. E. G. Straser and A. S. Kiremidjian, 'A modular, visual approach to damage monitoring for civil structures', *2nd int. workshop on structural control*, Hong Kong, 1996.
24. F. E. Udwadia, D. K. Sharma, and P. C. Shah, 'Uniqueness of damping and stiffness distributions in the identification of soil and structural systems', *J. applied mech.*,**45**, 180-187 (1978).
25. D. C. Zimmerman and M. Kaouk, 'Structural damage detection using a subspace rotation algorithm', *Proc. 33rd AIAA/ASME/ASCE/AHS structure, structural dynamics and materials conf.*, Dallas, TEX, 1992.

References

1. A. K. Ahmadi. *Application of System Identification in Mathematical Modeling of Buildings*. PhD thesis, Department of Civil Engineering, University of Pittsburgh, Pittsburgh, Pennsylvania, 1986.
2. J. L. Beck and L. S. Katafygiotis. Probabilistic system identification and health monitoring of structures. In *The Proceedings of The Tenth World Conference on Earthquake Engineering*, pages 3721–3726, Balkema Rotterdam, 1992.
3. J. L. Beck, M. W. Vanik, and L. S. Katafygiotis. Determination of stiffness changes from modal parameter changes for structural health monitoring. In *The Proceedings of The First World Conference on Structural Control*, Pasadena, CA, 1994.
4. J. S. Bendat and A. G. Piersol. *Random Data: Analysis and Measurement procedures, Second Edition*. John Wiley and Sons Inc., New Year, 1986.

5. A. Berman and E. J. Nagy. Improvements of a large analytical model using test data. *American Institute of Aeronautics and Astronautics*, 21:1168–1173, 1983.
6. J. C. Chen and J. A. Garba. On-orbit damage assessment for large space structures. *American Institute of Aeronautics and Astronautics*, 26:1119–1126, 1988.
7. A. K. Chopra. *Dynamics of Structures*. Prentice Hall, New Jersey, 1995.
8. C. R. Farrar, W. E. Baker, T. M. Bell, K. M. Cone, T. W. Darling, T. A. Duffey, A. Eklund, and A. Migliori. Dynamic characterization and damage detection in the I-40 bridge over the rio grande. Technical Report LA-12767-MS, Los Alamos National Laboratory, Los Alamos, New Mexico, 1994.
9. G. V. Garcia and N. Stubbs. Relative performance evaluation of pattern recognition models for nondestructive damage detection (ndd). In *The Proceeding of the 15th International Modal Analysis Conference, Orlando, FL*, pages 1822–1830, 1997.
10. J. He and D. J. Ewins. Compatibility of measured and predicted vibration modes in model improvement studies. *American Institute of Aeronautics and Astronautics*, 29:798–803, 1991.
11. F. M. Hemez. *Theoretical and Experimental Correlation between Finite Element Models and Modal Tests in the Context of Large Flexible Space Structures*. PhD thesis, University of Colorado, Boulder, Colorado, 1993.
12. M. Henrion. *Towards Efficient Probabilistic Diagnosis in Multiply Connected Belief Networks*, pages 385–409. John Wiley and Sons Inc., 1990.
13. M. Imregun and D. J. Ewins. An investigation into mode shape expansion techniques. In *The Proceedings of The 11th International Modal Analysis Conference, Kissimmee, Florida*, pages 168–175, 1993.
14. G. H. James, D. C. Zimmerman, C. R. Farrar, and S. W. Doebling. Current horizon for structural damage detection course. In *SEM short course held at the 15th IMAX conference, Orlando, Florida*, 1997.
15. A. M. Kabe. Stiffness matrix adjustment using mode data. *American Institute of Aeronautics and Astronautics*, 23:1431–1436, 1985.
16. D. C. Kammer. Optimum approximation for residual stiffness in linear system identification. *American Institute of Aeronautics and Astronautics*, 26:104–112, 1988.
17. M. Kaouk and D.C. Zimmerman. Structural damage assessment using a generalized minimum rank perturbation theory. In *The Proceeding of The 34th AIAA Structures, Structural Dynamics and Materials Conference, La Jolla, CA.*, 1993.
18. L. S. Katafygiotis. Treatment of model uncertainties in structural dynamics. Technical Report EERL 91-01, Earthquake Engineering Research Laboratory, California Institute of Technology, Pasadena, California, 1991.
19. J. M. Ricles and J. B. Kosmatka. Damage detection in elastic structures using vibratory residual forces and weighted sensitivity. *American Institute of Aeronautics and Astronautics*, 30:2310–2316, 1992.
20. S. W. Smith. *Damage Detection and Location in Large Space Trusses*. PhD thesis, Virginia Polytechnic Institute and State University, Blacksburg, Virginia, 1988.
21. S. W. Smith and C. A. Beattie. Simultaneous expansion and orthogonalization of measured modes for structure identification. *American Institute of Aeronautics and Astronautics*, AIAA-90-1218-CP:261–270, 1990.
22. S. W. Smith and C. A. Beattie. Secant-method adjustment for structural models. *American Institute of Aeronautics and Astronautics*, 29:119–126, 1991.

23. E. G. Straser and A. S. Kiremidjian. A modular, visual approach to damage monitoring for civil structures. In *The Second International Workshop on Structural Control, Hong Kong*, pages 532–544, 1996.
24. F. E. Udwadia, D. K. Sharma, and P. C. Shah. Uniqueness of damping and stiffness distributions in the identification of soil and structural systems. *Journal of Applied Mechanics*, 45:180–187, 1978.
25. D. C. Zimmerman and M. Kaouk. Structural damage detection using a subspace rotation algorithm. In *The Proceedings of The 33rd AIAA Structure, Structural Dynamics and Materials Conference, Dallas Texas*, pages 2341–2350, 1992.